Arabian Journal for Science and Engineering
https://doi.org/10.1007/s13369-025-10125-w

RESEARCH ARTICLE-CIVIL ENGINEERING

A New Approach for the Solution of One-Dimensional Consolidation Equation in Saturated Soils Under Various Time-Varying Loads

Rand Majid Rasool Zwayen[1] · Ahmad Reshad Noori[1] · Suleiman Khatrush[1] · Timuçin Alp Aslan[2]

Received: 23 November 2024 / Accepted: 11 March 2025

Abstract
A unified approach for solving the one-dimensional consolidation equation is introduced for the first time in geotechnical engineering. The one-dimensional consolidation partial differential equation is solved through a combined approach employing the complementary functions method (CFM) and Laplace transform. Using the coded program prepared in the FORTRAN, various time-varying loads are applied to different soil types to obtain the response of excess pore water pressure. The comparison demonstrated an excellent agreement, thus proving the effectiveness, applicability, and capability of the proposed approach in solving the governing canonical equations. The study's findings reveal that sand soil (high permeability) exhibits a less pronounced cyclic response under various cyclic loads compared to other soil types, whereas clay soil (low permeability) exhibits significant periodicity in its response. The investigation into the effect of soil properties on one-dimensional consolidation indicates that the dissipation of excess pore water pressure occurs relatively quickly in the case of highly permeable soils and gradually slows down as the soil permeability decreases. Due to the lower permeability of clay soil, the full dissipation of excess pore water pressure takes a much longer time compared to other soil types. Consequently, this process occurs over a more extended period in clay soil.

Keywords One-dimensional consolidation · Excess pore water pressure · Complementary functions method (CFM) · Cyclic loading · Laplace domain · Saturated soils

1 Introduction

Consolidation is a time-dependent process that involves stress, strain, and the passage of time, observed in saturated soils with fine particles. When a certain load is applied to the saturated soil, an increase in total stress occurs, causing a sudden rise in pore water pressure which gradually decreases with time. Terzaghi [1, 2] was the first to develop the theory of one-dimensional consolidation of soils. The theory was initially developed for sustained loading and does not account for cases involving cyclic loading. Subsequently, Schiffman [3] formulated an expression to determine excess pore water pressures in a soil layer subjected to different time-dependent loadings.

Consolidation is a crucial factor to consider in the stability analysis of columns, footings, or embankments constructed on saturated soft soils [4]. Due to the significance of cyclic loading applications in various fields such as railway, airport, and highway engineering, the behavior of roadbed soil or subgrade soil in geotechnical structures like these is influenced by the time-dependent nature of cyclic loading. Engineers encounter challenges with cyclic loads that the soils exposed, especially from moving vehicles on highways, leading to soil settlement. Several significant instances of cyclic loads are applied to the soil such as the impact of waves on coastal areas, the diverse stresses arising from machinery and equipment movement within the industrial floor, tidal changes affecting water levels, the dynamic loads experienced by

✉ Rand Majid Rasool Zwayen
randalgar3awi@gmail.com

Ahmad Reshad Noori
arnoori@gelisim.edu.tr

Suleiman Khatrush
sasmohamed@gelisim.edu.tr

Timuçin Alp Aslan
taslan@cu.edu.tr

[1] Department of Civil Engineering, Istanbul Gelisim University, Istanbul, Turkey

[2] Department of Civil Engineering, Çukurova University, Adana, Turkey

Published online: 05 April 2025

bridge supports, and the loads exerted by the wind on various structures. The presence of these cyclic loads in the field significantly differs from theoretical expectations based on static loads. Consequently, it becomes significant to investigate the impact of these cyclic loads, which contribute to soil settlement problems.

Many studies were previously conducted to examine the impact of various cyclic loadings on the process of one-dimensional consolidation. Wilson and Elgohary [5] obtained a theoretical solution for the consolidation process in a saturated soil layer under cyclic loading by using the integral transformation approach. The impact of cyclic loads, including sinusoidal, rectangular, and triangular loads, was analyzed by Xu et al. [6] based on Terzaghi's principle. Yuan-qiang et al. [7] presented a semi-analytical solution, investigating the effects of the same type of cyclic loads previously studied by Xu et al. [6]. Ying-chun and Kang-he [8] introduced a semi-analytical approach to address the one-dimensional consolidation problem, specifically taking into account the compressibility of soil during cyclic loading. Xie et al. [9] developed an analytical solution addressing the one-dimensional nonlinear consolidation behavior of soil under trapezoidal cyclic loading. Furthermore, Cai et al. [10] conducted a study to investigate similar loading effects, including other types of cyclic loads such as rectangular and triangular loads. Additionally, [11] developed an analytical solution to predict the excess pore water pressure in unsaturated soil under cyclic loading with square and triangular patterns. Many studies [12–14] were conducted to examine the effects of ramp loads on the consolidation process in soils. In addition to their work, Xie et al. [15] offered an analytical solution for the one-dimensional consolidation of soils induced by various pumping and loading types, such as cyclic pumping, step pumping, step loading, and continuous loading. Various numerical methods have been employed to examine the effects of time-dependent loading on one-dimensional consolidation. For instance, Hawlader et al. [16] and Satwik and Chakraborty [17] utilized the finite difference method. Müthing et al. [18] presented the haversine loading waveform, which includes rest periods, similar to the one reported by Razouki and Schanz [19]. A straightforward method was proposed by Chai et al. [20] for determining the one-dimensional consolidation settlement curve caused by intermittent cyclic loads based on the outcomes of finite element studies.

Laplace transform techniques were employed by various researchers to solve the governing equation of consolidation [21–24]. Additionally, Huang et al. [25] employed Laplace transform techniques to derive a series of analytical solutions for determining the excess pore water pressure. An analytical solution addressing the problem of one-dimensional consolidation of soil with double layers was presented by [26], utilizing the differential quadrature method and Laplace transform techniques, building upon the work of Xie [27]. Both the Laplace transform and the Crump inverse method were used to derive semi-analytical solutions for calculating pore water pressure and determining the degree of consolidation [28]. Moreover, [29] proposed a semi-analytical solution for the two-dimensional electro-osmotic consolidation of unsaturated, double-layered soil by utilizing Laplace transform techniques.

In recent years, this topic has gained great importance through studies that have focused on it. Semi-analytical solutions are obtained and verified through comparisons with experimental data, numerical models, and finite element method simulations by Tian et al. [30]. Chung et al. [31] presented the theoretical and experimental relationships between settlement and time. Different statistical methods were followed by Olek [32] to find the consolidation coefficient and end of primary consolidation based on laboratory data of pore water pressure and compression. More methods were used to test the swelling pressure of lime-stabilized bentonite soil, which is crucial for the stability of tunnel walls that use bentonite. Expansive soil settlement are a major cause of significant damage to highways, roads, and the protective shell of tunnels that use bentonite for stability [33].

The accuracy of correlations between undrained shear strength, compression index, and modulus of volumetric compressibility with index parameters was evaluated for Turkish clays [34]. Arab et al. [35] investigated the behavior of two different types of sand combined with plastic particles with an emphasis on compressibility, consolidation, and stress/strain response. Further, the study investigated how bentonite stabilizes these sands. Singh and Chakraborty [36] examined the consolidation behavior of unsaturated soil that is surrounded by semipermeable drainage boundaries and experiences nonlinear water flow. For both the air and water phases, the classical diffusion equations control the transient fluid flow process. Closed-form series solutions based on poroelasticity theory were developed to assess the steady-state and transient responses of total settlement and excess pore water pressure in saturated soils subjected to time-dependent loading [37].

Nonetheless, based on the best of the researchers' understanding and knowledge, solving the one-dimensional consolidation equation in the Laplace domain by the CFM has not yet been reported in the existing studies. The main goal of this paper is to tackle the present class of problems under any time-dependent load. For the first time in geotechnical engineering, this unified approach is implemented, paving the way for more advanced and efficient solutions.

It is worth mentioning that this unified approach has been successfully and effectively applied previously in many engineering problems [38–48]. Furthermore, previous studies [41, 42] have shown the efficiency and computational cost

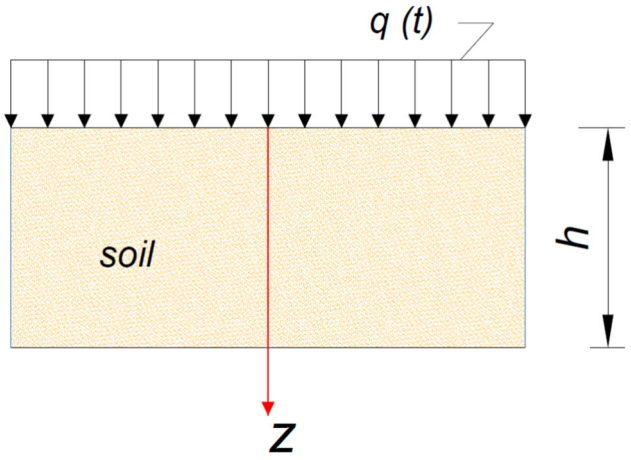

Fig. 1 One-dimensional consolidation

superiority of the suggested method over other numerical methods.

In the present paper, a proposed approach is presented for solving the one-dimensional consolidation equation and predicting excess pore water pressure variation with time is described. The Laplace transform concerning time is applied to solve the equation governing the one-dimensional consolidation equation, which is a partial differential equation, transforming it into an ordinary differential equation in the transformed domain. Then, by employing the CFM, the ordinary governing equation is simplified, allowing the boundary value problem to be transformed into an initial value problem. An efficient numerical method for inverse Laplace transform has been applied to convert the obtained results into the time domain. A FORTRAN program is developed to obtain the results of excess pore water pressure for eleven different soil types under six various time-dependent loads. Upon comparison with results from existing literature studies, it is observed that they exhibited good agreement. Furthermore, the effect of soil properties on the one-dimensional consolidation process is investigated by applying a constant load and five various cyclic loads to the same type of soil. Finally, the results are provided, and conclusions are drawn.

2 Materials and Method

2.1 Governing Equations of 1D Consolidation (Model Equations)

As per the theory of one-dimensional consolidation for porous media saturated with water (Fig. 1) suggested by Biot [49] under cyclic loads $q(t)$ applied to the surface's top, the one-dimensional consolidation problem's diffusion equation Eq. (1), which governs the dissipation of excess pore water pressure p_f over time t and depth z, can be described below [37]:

$$\frac{\partial p_f}{\partial t} = c_v \frac{\partial^2 p_f}{\partial z^2} - \gamma \frac{\partial q(t)}{\partial t} \tag{1}$$

where c_v represents the consolidation coefficient and γ denotes the efficiency of loading. The following equations, which represent the hydraulic and elastic characteristics of soil containing water, can be used to get the values of c_v and γ [37].

$$c_v = \frac{\frac{k_s}{\eta}}{\left[\frac{\alpha^2}{\left(K_b+\frac{4}{3}G\right)} + \frac{1}{M}\right]} \tag{2}$$

$$\gamma = \frac{\alpha M}{\left(K_b + \frac{4}{3}G + \alpha^2 M\right)} \tag{3}$$

where G denotes the porous medium's shear modulus, k_s represents intrinsic permeability, η refers to water's dynamic viscosity, and α represents the coefficient of Biot–Willis [50, 51] which can be expressed as follows:

$$\alpha = 1 - \frac{K_b}{K_s} \tag{4}$$

where K_b denotes the bulk modulus of soil (porous medium) and K_s the bulk modulus of a solid phase. The Biot poroelasticity coefficient is denoted as M Biot [51], can be determined using Eq. (5):

$$M = \frac{K_s}{\left[1 - \emptyset - \frac{K_b}{K_s} + \emptyset\frac{K_s}{K_f}\right]} \tag{5}$$

where $\emptyset$ denotes the porosity and K_f the bulk modulus of water.

2.2 Initial and Boundary Conditions

Initial and boundary conditions can be used to obtain the canonical equations that govern the one-dimensional consolidation problem and determine the excess pore water distribution as a function of time. Utilizing the method proposed in this study, the boundary value problem is resolved by converting it into an initial value problem. In the present study, the case of undrained conditions is considered with regard to the initial conditions. Under undrained conditions, neither water nor air escapes at the moment when the instantaneous load (total compaction stress) p^* is applied to saturated soil [52–54]. The initial conditions of the excess pore water pressure, as given by Lo et al. [55], can be described as follows:

$$p_f(z, 0) = \gamma p^* \tag{6}$$

Equation (1), representing the diffusion equation of the one-dimensional consolidation, this partial differential equation regards the dissipation of excess pore water pressure in terms of p_f as a dependent variable, relying on the independent variables time t and depth z. As such, the variable p_f undergoes two derivatives for depth z. and one derivative with respect to time t. Therefore, two boundary conditions need to be determined to solve Eq. (1). These conditions usually arise from various depths within the soil layer, where the values of excess pore pressure are known. These boundary conditions can take the form of either one-way drainage or two-way drainage, contingent on the specific layers positioned above and below the saturated layer in which the consolidation occurs. In the present study, double drainage is considered. This means that pore pressure, escaping from the soil pores, is drained in two directions: upwards, toward the upper drainage boundary, and downwards, toward the lower drainage boundary [56].

The boundary conditions of the problem can be expressed as follows [55]:

$$p_f(0,\, t) = 0 \tag{7}$$

$$p_f(h,\, t) = 0 \tag{8}$$

The boundary conditions considered permeable surfaces at both the bottom surface ($z = 0$) and the top surface ($z = h$). It is assumed that the height h is permeable to water, allowing water to flow freely through these boundaries.

Also, for the imposed load value at the initial conditions when $t = 0$, the q value is determined in Eq. (9);

$$q(0) = -p^* \tag{9}$$

2.3 The Theoretical Solution of the One-dimensional Consolidation Equation

2.3.1 Application of the Laplace Transform

The Laplace transform is applied to Eq. (1), which is a partial differential equation PDE and converted to an ordinary differential equation ODE. The Laplace transform techniques ($\mathcal{L}$ []) of a time-domain function, which is described by Spiegel [57], are applied to the first and second derivatives in Eq. (1). Taking into account the initial conditions of the equation, each term in Eq. (1) can be transformed into the Laplace domain as follows:

$$\mathcal{L}\left[\frac{\partial p_f}{\partial t}\right] = s\overline{p}_f(s) - p_f(0) \tag{10}$$

$$\mathcal{L}\left[\frac{\partial^2 p_f}{\partial z^2}\right] = \frac{d^2\overline{p}_f}{dz^2} \tag{11}$$

$$\mathcal{L}\left[\frac{\partial q}{\partial t}\right] = s\overline{q}(s) - q(0) \tag{12}$$

where s denotes the Laplace transform parameter and $\bar{\cdot}$ represents the Laplace transformation of the quantities.

Substituting the initial condition of excess pore water pressure as stated in Eq. (6) into Eq. (10), and similarly, substituting the initial value of the imposed load as expressed in Eq. (9) into Eq. (12), results in:

$$\mathcal{L}\left[\frac{\partial p_f}{\partial t}\right] = s\overline{p}_f(s) + \gamma p^* \tag{13}$$

$$\mathcal{L}\left[\frac{\partial q(t)}{\partial t}\right] = s\overline{q}(s) + p^* \tag{14}$$

Accordingly, the ordinary differential equation governing one-dimensional consolidation can now be written in the Laplace domain, taking the following forms:

$$s\overline{p}_f(s) + \gamma p^* = c_v\frac{d^2\overline{p}_f}{dz^2} - \gamma\left(s\overline{q}(s) + p^*\right) \tag{15}$$

$$s\overline{p}_f(s) + \gamma p^* = c_v\frac{d^2\overline{p}_f}{dz^2} - \gamma s\overline{q}(s) - \gamma p^* \tag{16}$$

$$s\overline{p}_f(s) = c_v\frac{d^2\overline{p}_f}{dz^2} - \gamma s\overline{q}(s) - 2\gamma p^* \tag{17}$$

$$c_v\frac{d^2\overline{p}_f}{dz^2} = s\overline{p}_f(s) + \gamma s\overline{q}(s) + 2\gamma p^* \tag{18}$$

By simplifying Eq. (18), Eq. (19) is obtained;

$$\frac{d^2\overline{p}_f}{dz^2} = \frac{1}{c_v}\left(s\overline{p}_f(s) + \gamma s\overline{q}(s) + 2\gamma p^*\right) \tag{19}$$

2.3.2 Application of the CFM

As mentioned earlier, the solution proposed in this study has been successfully applied to many structural mechanics problems. However, this is the first time it has been applied in geotechnical engineering to address the one-dimensional consolidation problem. To examine the excess pore water pressure response in one-dimensional consolidation, the CFM is applied to the obtained governing ordinary differential Eq. (19) in the transformed domain. The basic idea behind this approach is to streamline two-point boundary value problems by transforming them into initial value problems. When applied to the current type of problem, it proves to be an efficient and effective method.

Letting $\overline{p}_f = y_1$ and $\frac{d\overline{p}_f}{dz} = y_2$ yields

$$y_1' = \frac{dy_1}{dz} = y_2 \tag{20}$$

$$y_2' = \frac{dy_2}{dz} = \frac{d^2\overline{p}_f}{dz^2} = \frac{1}{c_v}\left(s\overline{p}_f(s) + \gamma s\overline{q}(s) + 2\gamma p^*\right) \quad (21)$$

So the equations governing the one-dimensional consolidation are obtained in canonical form Eqs. (22) and (23) as given below:

$$\frac{dy_1}{dz} = y_2 \quad (22)$$

$$\frac{dy_2}{dz} = \frac{1}{c_v}\left(s\overline{p}_f(s) + \gamma s\overline{q}(s) + 2\gamma p^*\right) \quad (23)$$

It is important again to mention that the canonical equations derived in this study are introduced for the first time. The objective is to study the behavior of excess pore water pressure during a one-dimensional consolidation process.

2.4 Time-varying External Loads and Their Laplace Transforms

In this study, various cyclic loads are exerted for different soil types, and their impact on the soil's behavior is thoroughly investigated using the method proposed in this study. The applied cyclic loads are transformed into the Laplace domain and implemented within the program prepared and coded in the FORTRAN.

2.4.1 Constant Type Loading $q_1(t)$

The imposed load $q_1(t)$ shown in Fig. 2a is:

$$q_1(t) = -p^* \quad (24)$$

The Laplace transform of Eq. (24), which is given by Spiegel [57]:

$$\overline{q_1}(s) = \frac{1}{s} \quad (25)$$

2.4.2 Cosine-wave Type Cyclic Loading $q_2(t)$

The imposed load $q_2(t)$ shown in Fig. 2b is:

$$q_2(t) = -p^* cos^2\left(\frac{\omega t}{2}\right) \quad (26)$$

The angular frequency of the cosine wave, denoted as ω, is expressed as $\omega = 2\,\pi\, f$, where f represents the frequency in Hertz and is calculated as $\frac{1}{T}$. Consequently, substituting $\frac{1}{T}$ for f yields $\omega = \frac{2\pi}{T}$. Assuming $T = a$, where T represents the time of period, the expression $\omega = \frac{2\pi}{a}$ can be put in Eq. (26). Consequently, the cosine-wave type cyclic loading equation in the Laplace domain can be obtained:

$$\overline{q_2}(s) = -p^*\left[\frac{\left(2\pi^2 + a^2s^2\right)}{4\pi^2 s + a^2 s^3}\right] \quad (27)$$

2.4.3 Square-wave Type Cyclic Loading $q_3(t)$

The imposed load $q_3(t)$ is shown in Fig. 2c. The equation representing the square wave type is derived in the Laplace domain after applying the Laplace transform to the periodic load function mentioned in [57]:

$$\overline{q_3}(s) = -p^*\left[\frac{\left(1 - e^{-as}\right)}{(s)\left(1 - e^{-2as}\right)}\right] \quad (28)$$

2.4.4 Triangle-wave Type Cyclic Loading $q_4(t)$:

The imposed load $q_4(t)$ is shown in Fig. 2d. After applying the Laplace transform to the periodic load function, the equation representing the square wave type is obtained in the Laplace domain:

$$\overline{q_4}(s) = \frac{-p^*}{as^2}\left[-as + \frac{(e^{as} - 1)}{(e^{as} + 1)}\right] \quad (29)$$

2.4.5 Half-rectified Sine Wave Type Cyclic Loading $q_5(t)$

The imposed load $q_5(t)$ is shown in Fig. 2e. The equation representing the half-rectified sine wave type is derived in the Laplace domain after applying the Laplace transform to the periodic load function as below:

$$\overline{q_5}(s) = -p^*\left[\frac{\pi a}{\left(a^2s^2 + \pi^2\right)\left(1 - e^{-as}\right)}\right] \quad (30)$$

2.4.6 Saw Tooth-Wave Type Cyclic Loading $q_6(t)$

The imposed load $q_6(t)$ is shown in Fig. 2f. The equation representing the saw tooth wave type is derived in the Laplace domain after applying the Laplace transform to the periodic load function as below:

$$\overline{q_6}(s) = -p^*\left[\frac{1}{\left(as^2\right)} - \frac{e^{-as}}{s\left(1 - e^{-as}\right)}\right] \quad (31)$$

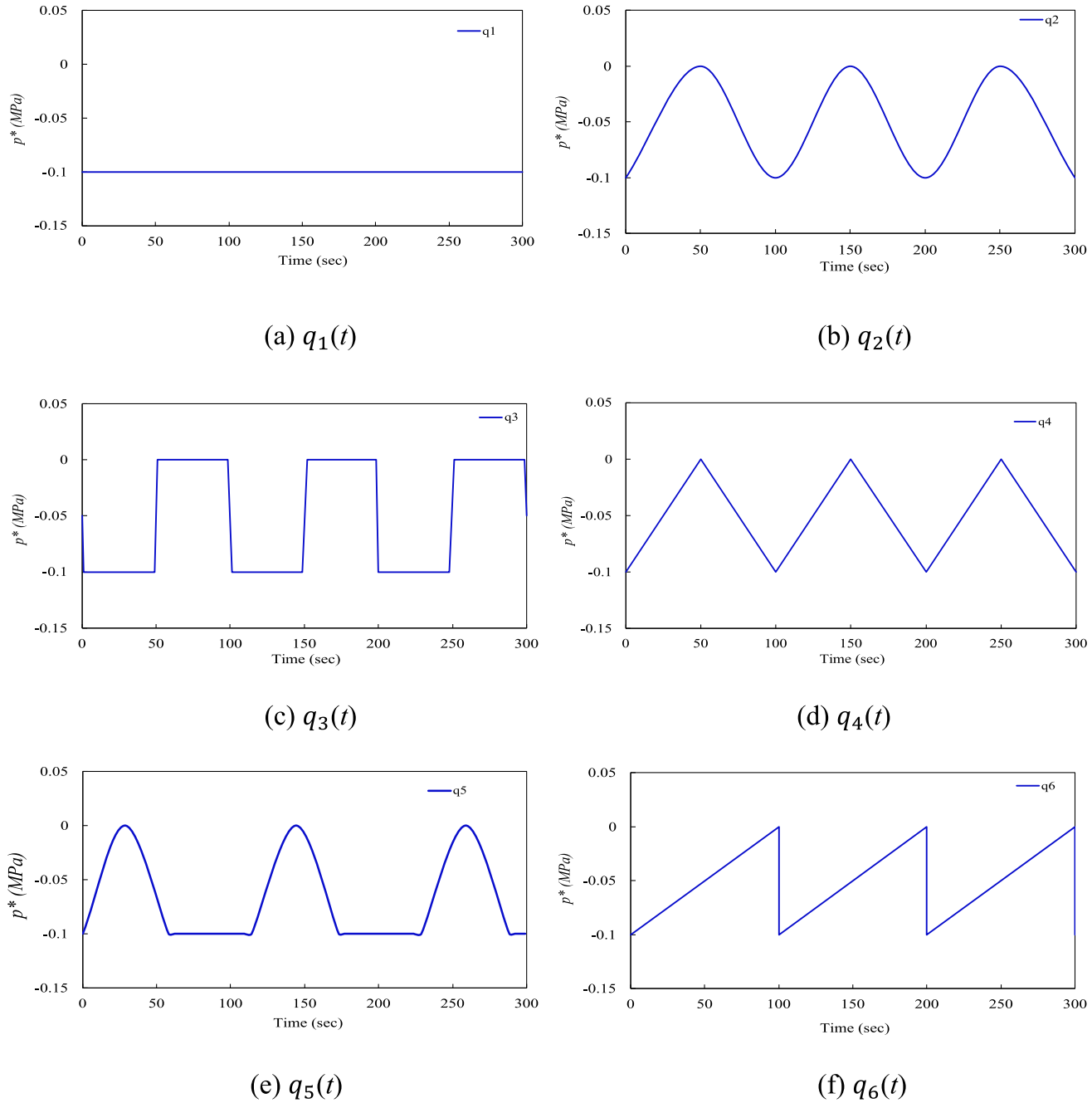

Fig. 2 Time-varying applied loads **a** constant type load $q_1(t)$, **b** cosine-wave type cyclic load $q_2(t)$, **c** square-wave type cyclic load $q_3(t)$, **d** triangle-wave type cyclic load $q_4(t)$, **e** half-rectified sine wave type cyclic load $q_5(t)$, and **f** saw tooth-wave type cyclic load $q_6(t)$

3 Results and Discussion

In this section, the values of excess pore water pressure that vary with time are addressed for eleven different types of soils subjected to six different loading cases; constant $q_1(t)$ loading or five different cyclic $q_2(t)$, $q_3(t)$, $q_4(t)$, $q_5(t)$ and $q_6(t)$ loading as illustrated in Fig. 2. The canonical Eqs. (22) and (23) derived in the Laplace domain have been integrated into the prepared FORTRAN programming language. In this study, the inverse Laplace transform is utilized to convert the outcomes acquired in the Laplace domain into the time domain, thereby obtaining the resulting excess pore water pressure. All operations are carried out with double precision in the program. The hydraulic and elastic parameters of both the solid particles and water that are used in the present study are summarized in Table 1.

In the current research, necessary parameters for numerical calculations like porosity $\emptyset$, soil bulk modulus K_b, shear

Table 1 Soil sample height, applied load, as well as the hydraulic and elastic parameters of both the solid particles and water [55, 58, 59]

Parameters	Value
Soil sample height	$h = 1\text{m}$
Bulk modulus of solid	$K_s = 35$ GPa
Bulk modulus of water	$K_f = 2.25$ GPa
Dynamic viscosity of water	$\eta = 0.001\ N_s/m^2$
Applied load	$p* = 0.\ 1$ MPa

modulus G, and intrinsic permeability k_s are employed for 11 different classes of soil texture which are presented in Table 2.

For the parametric studies in this work, values for M, α, γ, and c_v are computed using the parameters outlined in Table 1 and Table 2, applying Eqs. (2)–(5). These calculated values are listed in Table 3.

3.1 Validation

In order to validate the accuracy of the proposed solution, a comparison is conducted between the dimensionless excess pore water pressure ${}^{p_f}/_{p^*}$ results obtained from the proposed method in the present study and those obtained by Deng et al. [37]. These comparisons are carried out for two types of saturated soil, sand, and clay, subjected to various external time-varying loads.

The results of ${}^{p_f}/_{p^*}$ obtained for saturated sand soil subjected to three types of external time-varying loads are shown in Fig. 3 for (a) constant type load $q_1(t)$, (b) cosine-wave type cyclic load $q_2(t)$, and (c) triangle-wave type cyclic load $q_4(t)$. From Fig. 3, it is observed that the ${}^{p_f}/_{p^*}$ results for case $q_1(t)$ obtained in this study overlap with those obtained by Deng et al. [37]. Additionally, it can be seen that the results obtained in this study for cases $q_2(t)$ and $q_4(t)$ are in harmony with the results obtained by Deng et al. [37].

The results of ${}^{p_f}/_{p^*}$ obtained from this study are compared with those obtained by Deng et al. [37] for saturated clay soil subjected to three types of external time-varying loads as graphed and shown in Fig. 4 for (a) cosine-wave type cyclic load $q_2(t)$ (b) square-wave type cyclic load $q_3(t)$, and (c) triangle-wave type cyclic load $q_4(t)$. In Fig. 4, it is also observed that the results obtained by the proposed method completely match those of Deng et al. [37], demonstrating an excellent agreement.

3.2 Numerical Applications and Discussion

The impact of a constant load $q_1(t)$ and five different cyclic loads cosine-wave type cyclic load $q_2(t)$, square-wave type cyclic load $q_3(t)$, triangle-wave type cyclic load $q_4(t)$, half-rectified sine wave type cyclic load $q_5(t)$, and saw tooth-wave type cyclic load $q_6(t)$ applied to the same type of soil is examined. The dimensionless excess pore water pressure results obtained in the time domain for 11 types of soil are carried out by applying the canonical Eqs. (22) and (23) derived in this study in the Laplace domain within the prepared program. Hence, the resulting response of ${}^{p_f}/_{p^*}$ for sand, loamy sand, sandy loam, loam, silt loam, sandy clay loam, clay loam, silty clay loam, sandy clay, silty clay, and clay soils of which their properties are presented in Table 1 and Table 2 is investigated. Therefore, the variation of ${}^{p_f}/_{p^*}$ under any of the assigned applied types of loads for each one of the prescribed types of soil is graphically plotted with a time span of 100 to 1000 s.

The results for ${}^{p_f}/_{p^*}$ obtained from the present study under the effect of static load $q_1(t)$ and five different cyclic

Table 2 Porosity Ø, soil bulk modulus K_b, shear modulus G, and intrinsic permeability k_s for 11 different soil texture classes [60–62]

Soil texture class	Porosity Ø	Soil bulk modulus $K_b(MPa)$	Shear modulus$G$ (MPa)	Intrinsic permeability $k_s(m^2)$
Sand	0.437	35.3	13.3	5.946×10^{-12}
Loamy sand	0.437	29.9	11.3	1.730×10^{-12}
Sandy loam	0.453	25.4	9.3	7.334×10^{-13}
Loam	0.463	17.6	6.3	3.738×10^{-13}
Silt loam	0.501	16.2	5.5	1.925×10^{-13}
Sandy clay loam	0.398	23.8	9.1	1.218×10^{-13}
Clay loam	0.464	13.7	5.7	6.513×10^{-14}
Silty clay loam	0.471	12.3	4.3	4.247×10^{-14}
Sandy clay	0.430	20.7	8.0	3.398×10^{-14}
Silty clay	0.479	11.5	4.1	2.548×10^{-14}
Clay	0.475	4.5	2.4	1.699×10^{-14}

Table 3 The values of parameters M, α, γ, and c_v of 11 different soil texture classes

Soil texture class	Biot poroelasticity coefficient M (Pa)	Coefficient of Biot–Willis α	The loading efficiency γ	Coefficient of consolidation $c_v\left(m^2/sec\right)$
Sand	4.76×10^9	0.998991429	0.989947587	3.12×10^{-1}
Loamy sand	4.76×10^9	0.999145714	0.991463943	7.72×10^{-2}
Sandy loam	4.61×10^9	0.999274286	0.992574927	2.75×10^{-2}
Loam	4.52×10^9	0.999497143	0.994778608	9.67×10^{-3}
Silt loam	4.22×10^9	0.999537143	0.994911010	4.51×10^{-3}
Sandy clay loam	5.15×10^9	0.999320000	0.993741113	4.35×10^{-3}
Clay loam	4.51×10^9	0.999608571	0.995689750	1.38×10^{-3}
Silty clay loam	4.46×10^9	0.999648571	0.996316268	7.63×10^{-4}
Sandy clay	4.82×10^9	0.999408571	0.994117570	1.06×10^{-3}
Silty clay	4.39×10^9	0.999671429	0.996475352	4.31×10^{-4}
Clay	4.42×10^9	0.999871429	0.998389917	1.31×10^{-4}

loads for sand, loamy sand, and sandy loam soil are compared in (Figs. 5, 6 and 7) respectively with time span of 100 s. To better examine the response of p_f/p^* under various time-varying loads, this time interval is divided into periods of 10 s.

In terms of the load functions encountered as illustrated in (Figs. 5, 6), it becomes apparent that the p_f/p^* values reach their greatest values under square-wave type cyclic load function $q_3(t)$ among the various applied load functions in sand and loamy sand soil.

For sandy loam as observed in Fig. 7, it becomes apparent that the p_f/p^* values under the half-rectified sine wave type cyclic load function $q_5(t)$ take the largest value and are close to the p_f/p^* values under the square-wave type cyclic load function $q_3(t)$.

The results of p_f/p^* under various external time-varying loads for loam, silt loam, and sandy clay loam soils are depicted in (Figs. 8, 9 and 10) respectively with a time span of 200 s, while for clay loam, silty clay loam, and sandy clay, the results of p_f/p^* are further compared under various external time-varying loads with time span of 500 s as illustrated in (Figs. 11, 12 and 13) respectively. From (Figs. 8, 9, 10, 11, 12 and 13) for loam, silt loam, sandy clay loam, clay loam, silty clay loam, and sandy clay soils, it can be observed that the greatest p_f/p^* values occur under the half-rectified sine wave type cyclic load function $q_5(t)$.

The p_f/p^* values for silty clay and clay soils are also compared under various time-varying external loads with time span of 1000 s allowing longer time for more dissipation of excess pore water pressure, and illustrated in Figs. 14 and 15, respectively. In the case of silty clay, the greatest p_f/p^* values occur under the half-rectified sine wave type cyclic load function, whereas for clay soil, the graphs of p_f/p^* values oscillate at approximately the same values in terms of load functions.

In Fig. 16, the resulting response of p_f/p^* for sand, loamy sand, sandy loam, loam, silt loam, sandy clay loam, clay loam, silty clay loam, sandy clay, silty clay, and clay soils is examined under constant load $q_1(t)$ with time span of 1000 s.

As seen in Fig. 16, the value of p_f/p^* changes over time in different soil types has been found to be gradually decreasing. Since the permeability of sand soils is high, the p_f/p^* disperses and dissipates faster than in other soil types. As the permeability of the soil is getting lower, the full dissipation of p_f/p^* takes longer.

However, to better understand the behavior and response of p_f/p^*, three different soil types such as sand, sandy clay, and clay are examined under four various time-dependent loads constant load $q_1(t)$, cosine-wave type cyclic load $q_2(t)$, square-wave type cyclic load $q_3(t)$, and triangle-wave type cyclic load $q_4(t)$ as illustrated in Fig. 17. The time span for each type is taken as 1000 s. In Fig. 17a, it has been observed that the excess pore water pressure under the constant load $q_1(t)$ is completely dissipated in sand soil, while it is not completely dissipated in clay soil. Due to its high permeability, sand soil exhibits a faster dissipation of the p_f/p^* value compared to other soil types. Conversely, clay soils, with their low permeability, experience a slower dissipation of p_f/p^*, necessitating a relatively longer duration for this phenomenon to occur. This curve is similar to Terzaghi's exact solution in the clay soil.

In Fig. 17b, c, and d, it is noted that at 1000 s, the dissipation of excess pore water pressure in the sand graph is nearly to complete, while the periodic response persists in clay and sandy clay soils. Furthermore, oscillations diminish below zero with the passage of time.

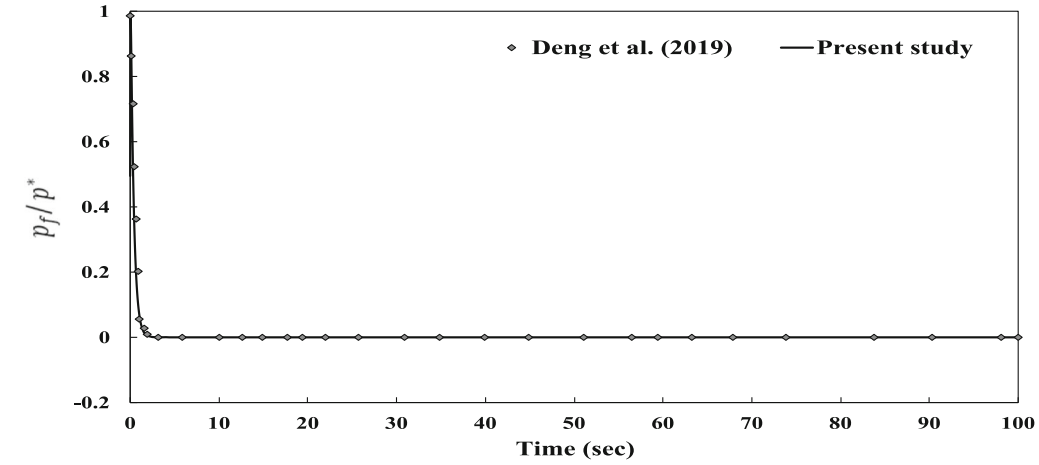

(a)

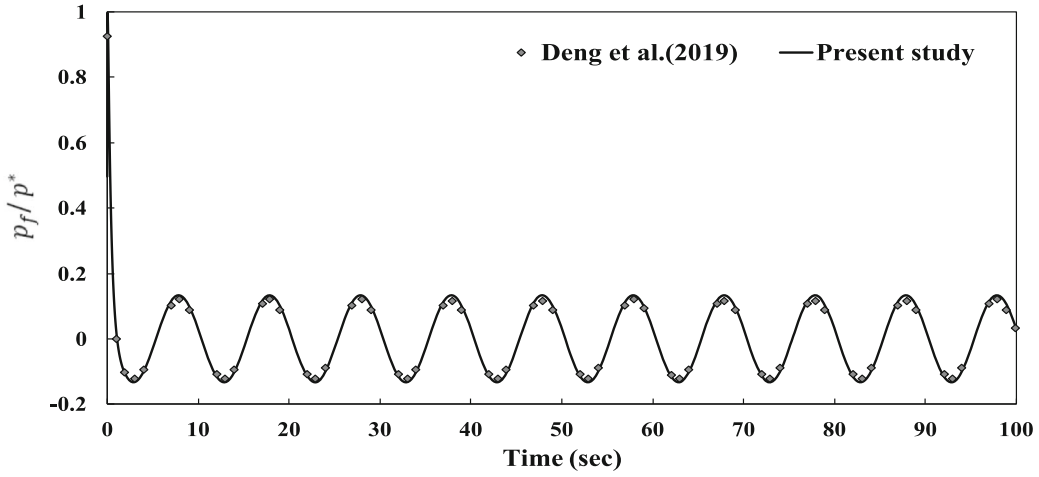

(b)

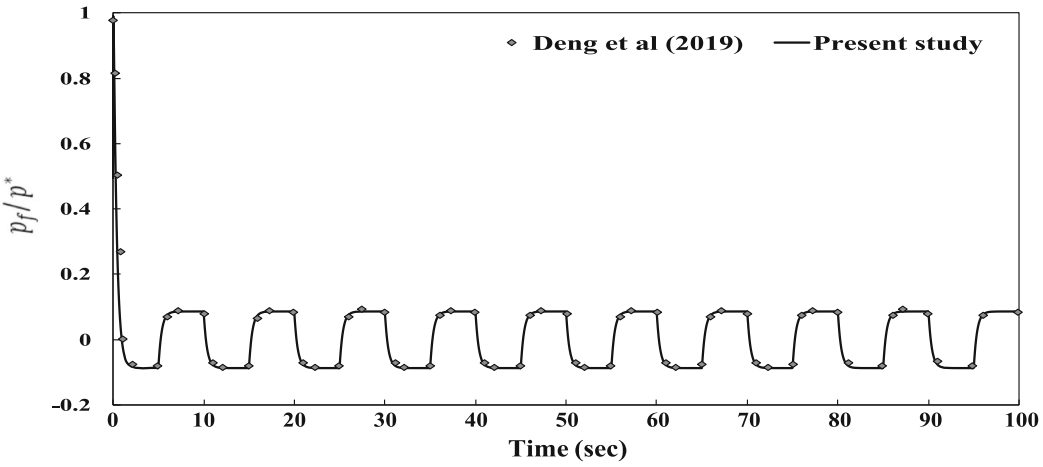

(c)

Fig. 3 A comparison between the results of dimensionless excess pore water pressure p_f/p^* obtained from the present study and those obtained by Deng et al. [37] for saturated sand soil under time-varying applied loads **a** constant type load $q_1(t)$, **b** cosine-wave type cyclic load $q_2(t)$, and **c** triangle-wave type cyclic load $q_4(t)$

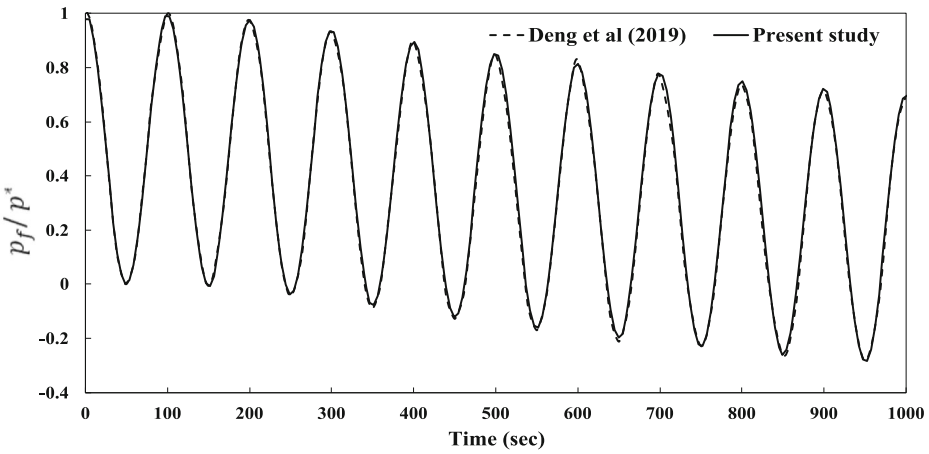

(a)

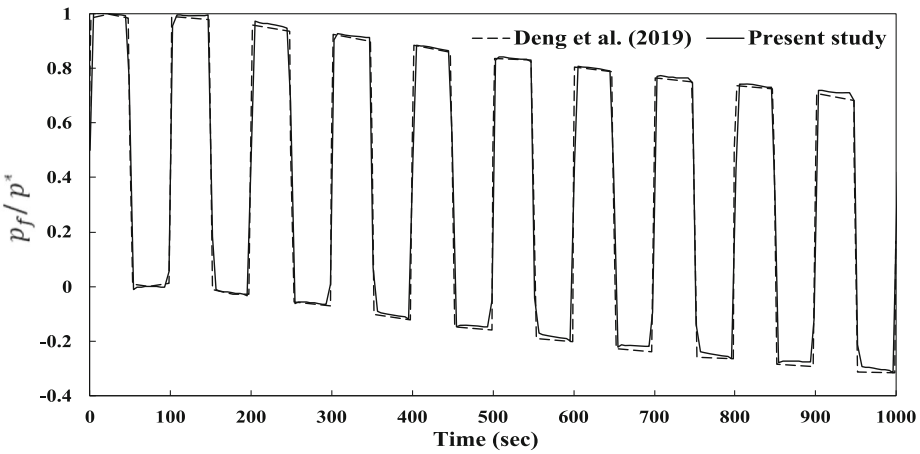

(b)

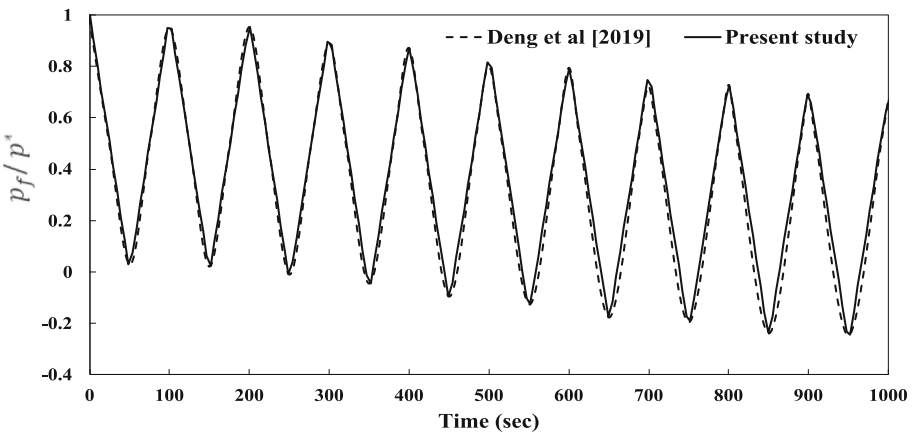

(c)

Fig. 4 A comparison between the results of dimensionless excess pore water pressure p_f/p^* obtained from the present study and those obtained by Deng et al. [37] for saturated clay soil under time-varying applied loads **a** cosine-wave type cyclic load $q_2(t)$ **b** square-wave type cyclic load $q_3(t)$, and **c** triangle-wave type cyclic load $q_4(t)$

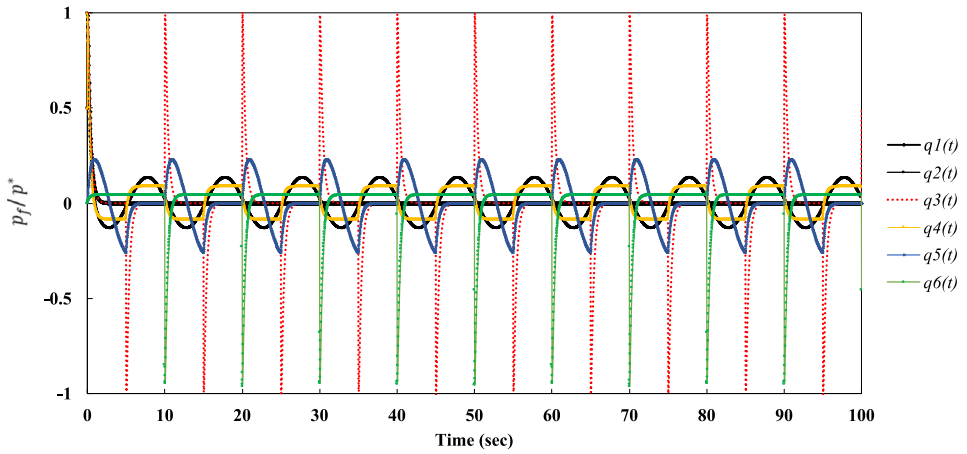

Fig. 5 A comparison of the results of dimensionless excess pore water pressure with time for saturated sand soil under constant type load $q_1(t)$, cosine-wave type cyclic load $q_2(t)$, square-wave type cyclic load $q_3(t)$, triangle-wave type cyclic load $q_4(t)$, half-rectified sine wave type cyclic load $q_5(t)$, and saw tooth-wave type cyclic load $q_6(t)$

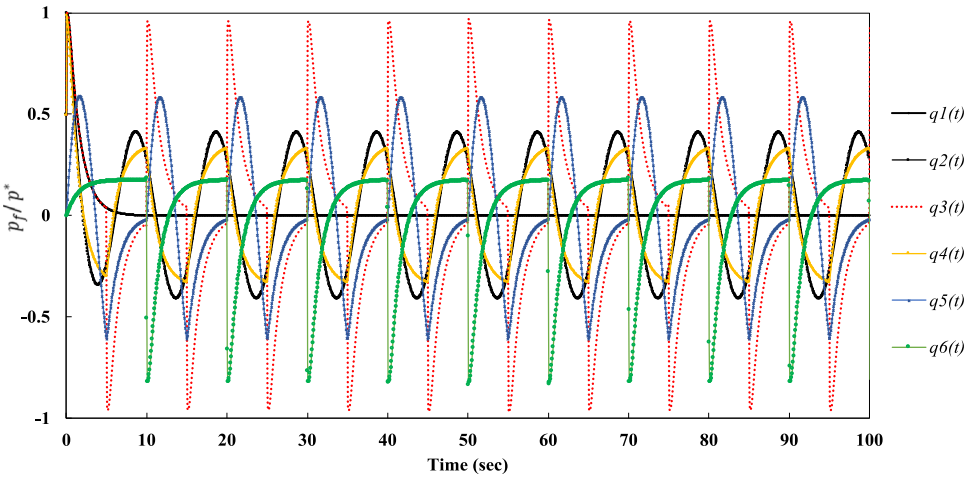

Fig. 6 A comparison of the results of dimensionless excess pore water pressure with time for saturated loamy sand soil under constant type load $q_1(t)$, cosine-wave type cyclic load $q_2(t)$, square-wave type cyclic load $q_3(t)$, triangle-wave type cyclic load $q_4(t)$, half-rectified sine wave type cyclic load $q_5(t)$, and saw tooth-wave type cyclic load $q_6(t)$

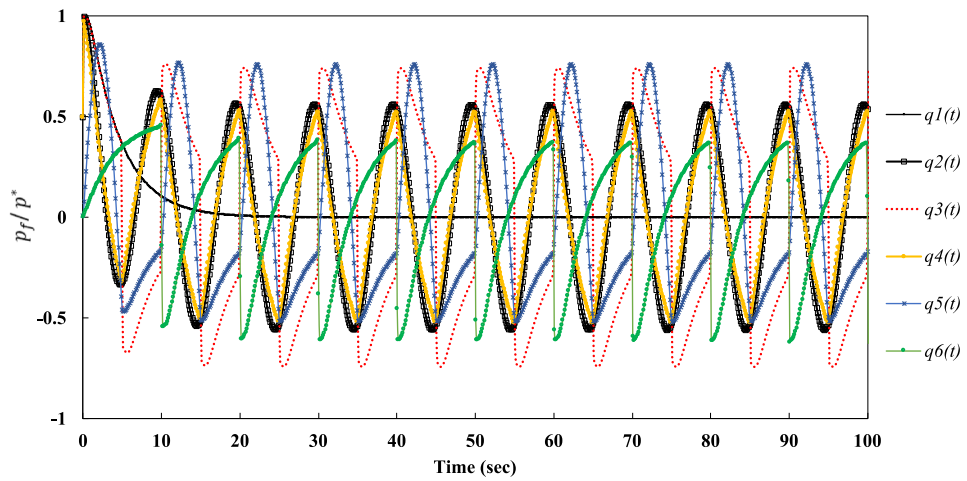

Fig. 7 A comparison of the results of dimensionless excess pore water pressure with time for saturated sandy loam soil under constant type load $q_1(t)$, cosine-wave type cyclic load $q_2(t)$, square-wave type cyclic load $q_3(t)$, triangle-wave type cyclic load $q_4(t)$, half-rectified sine wave type cyclic load $q_5(t)$, and saw tooth-wave type cyclic load $q_6(t)$

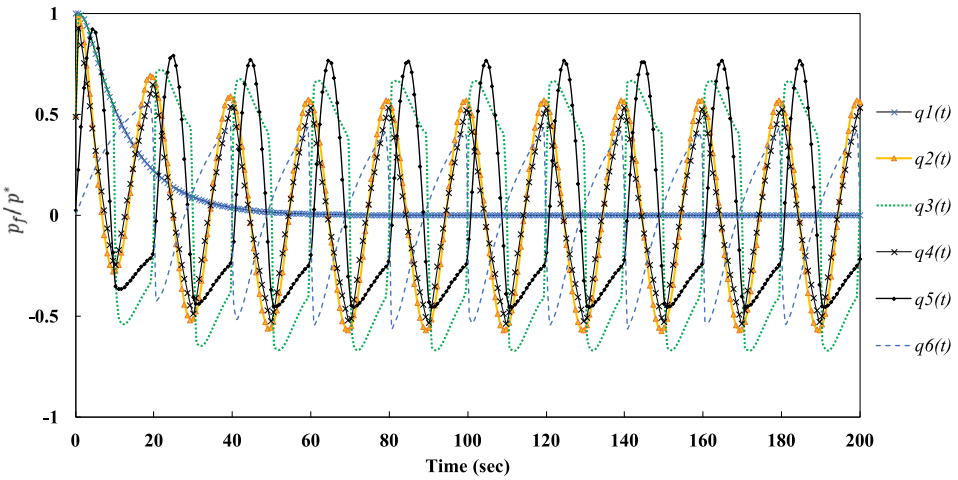

Fig. 8 A comparison of the results of dimensionless excess pore water pressure with time for saturated loam soil under constant type load $q_1(t)$, cosine-wave type cyclic load $q_2(t)$, square-wave type cyclic load $q_3(t)$, triangle-wave type cyclic load $q_4(t)$, half-rectified sine wave type cyclic load $q_5(t)$, and saw tooth-wave type cyclic load $q_6(t)$

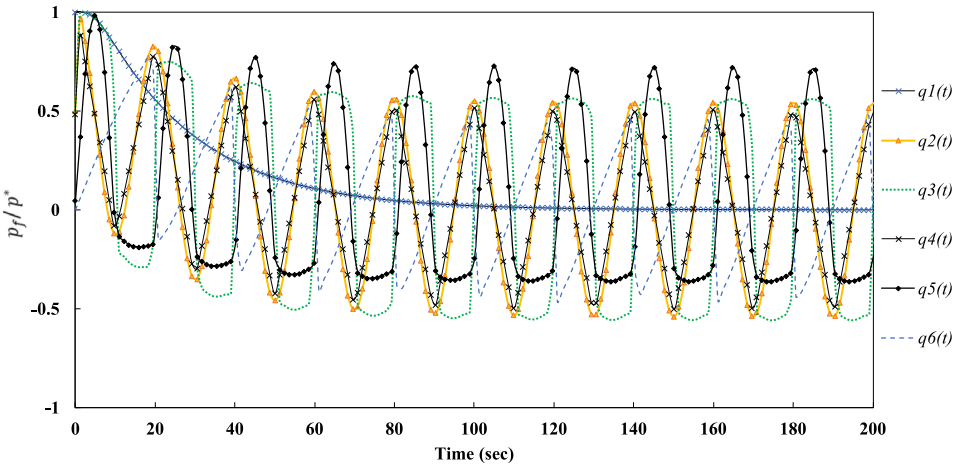

Fig. 9 A comparison of the results of dimensionless excess pore water pressure with time for saturated silt loam soil under constant type load $q_1(t)$, cosine-wave type cyclic load $q_2(t)$, square-wave type cyclic load $q_3(t)$, triangle-wave type cyclic load $q_4(t)$, half-rectified sine wave type cyclic load $q_5(t)$, and saw tooth-wave type cyclic load $q_6(t)$

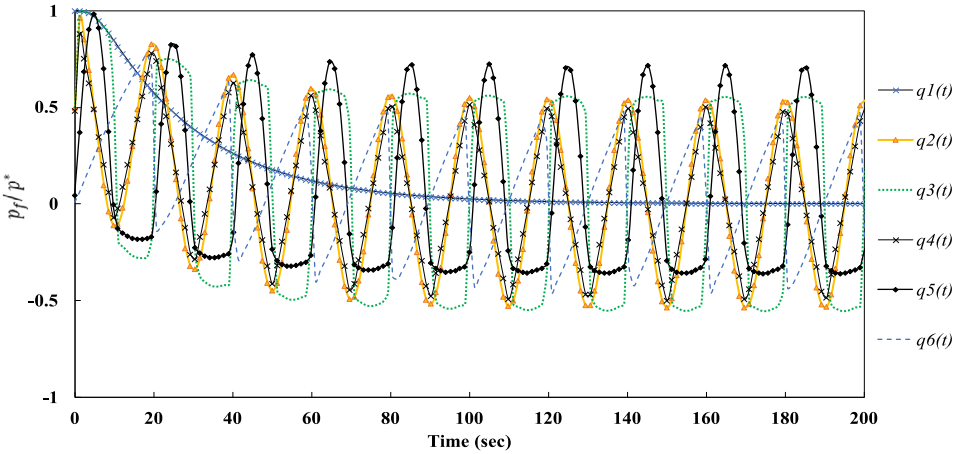

Fig. 10 A comparison of the results of dimensionless excess pore water pressure with time for saturated sandy clay loam soil under constant type load $q_1(t)$, cosine-wave type cyclic load $q_2(t)$, square-wave type cyclic load $q_3(t)$, triangle-wave type cyclic load $q_4(t)$, half-rectified sine wave type cyclic load $q_5(t)$, and saw tooth-wave type cyclic load $q_6(t)$

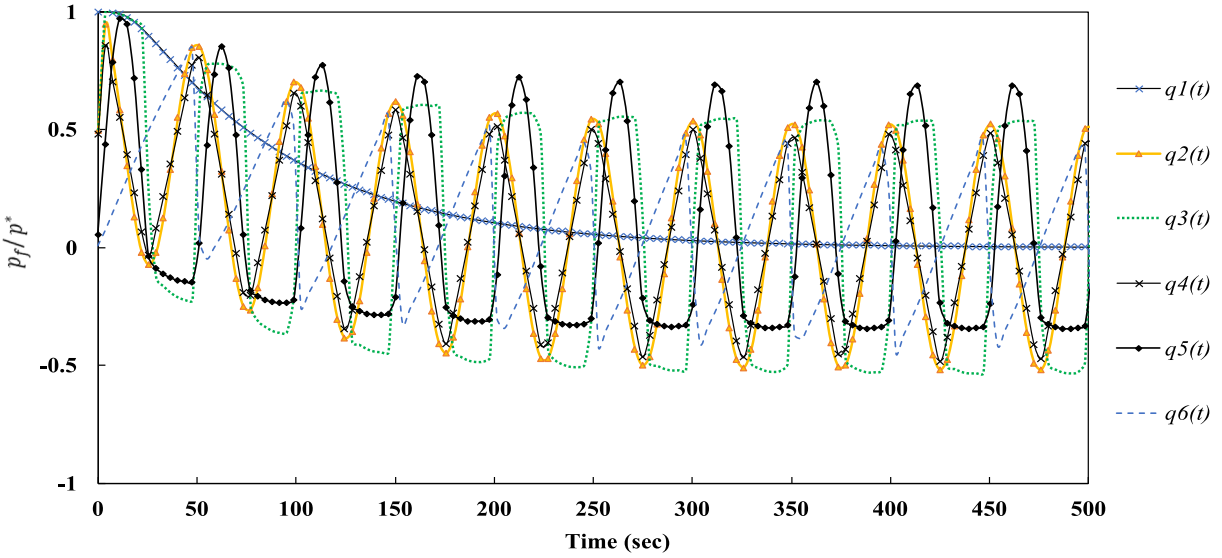

Fig. 11 A comparison of the results of dimensionless excess pore water pressure with time for saturated clay loam soil under constant type load $q_1(t)$, cosine-wave type cyclic load $q_2(t)$, square-wave type cyclic load $q_3(t)$, triangle-wave type cyclic load $q_4(t)$, half-rectified sine wave type cyclic load $q_5(t)$, and saw tooth-wave type cyclic load $q_6(t)$

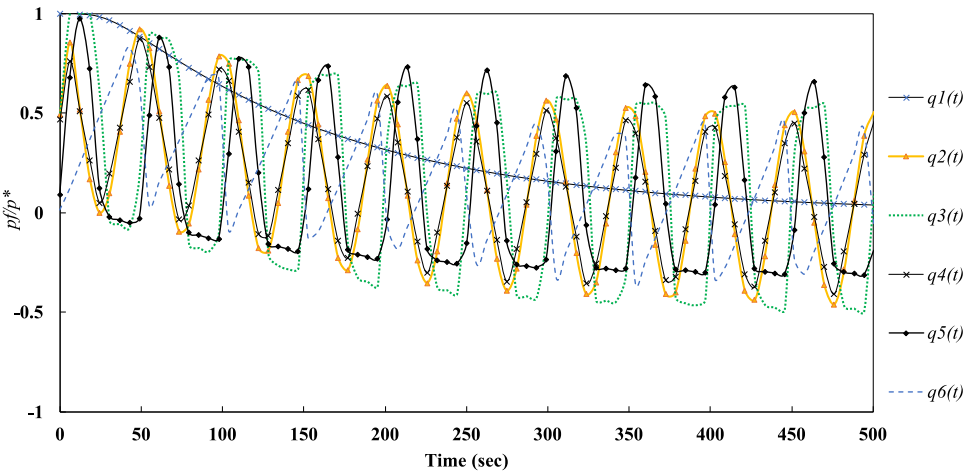

Fig. 12 A comparison of the results of dimensionless excess pore water pressure with time for saturated silty clay loam soil under constant type load $q_1(t)$, cosine-wave type cyclic load $q_2(t)$, square-wave type cyclic load $q_3(t)$, triangle-wave type cyclic load $q_4(t)$, half-rectified sine wave type cyclic load $q_5(t)$, and saw tooth-wave type cyclic load $q_6(t)$

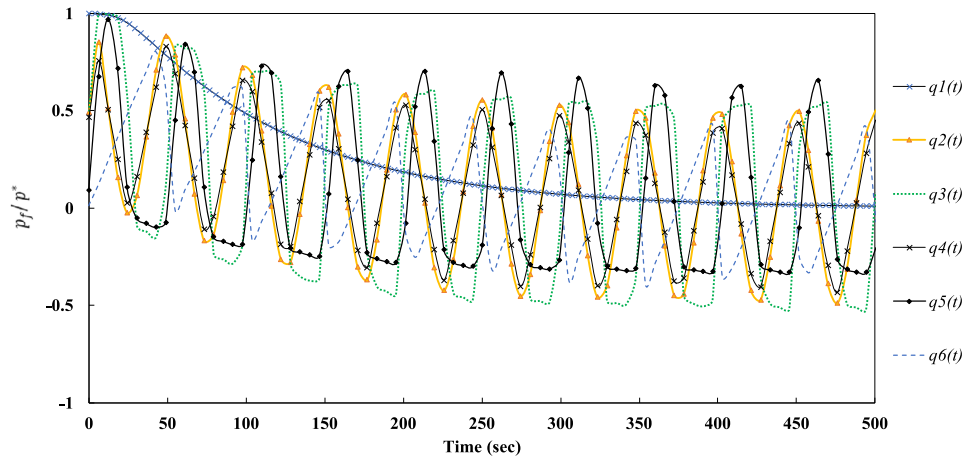

Fig. 13 A comparison of the results of dimensionless excess pore water pressure with time for saturated sandy clay soil under constant type load $q_1(t)$, cosine-wave type cyclic load $q_2(t)$, square-wave type cyclic load $q_3(t)$, triangle-wave type cyclic load $q_4(t)$, half-rectified sine wave type cyclic load $q_5(t)$, and saw tooth-wave type cyclic load $q_6(t)$

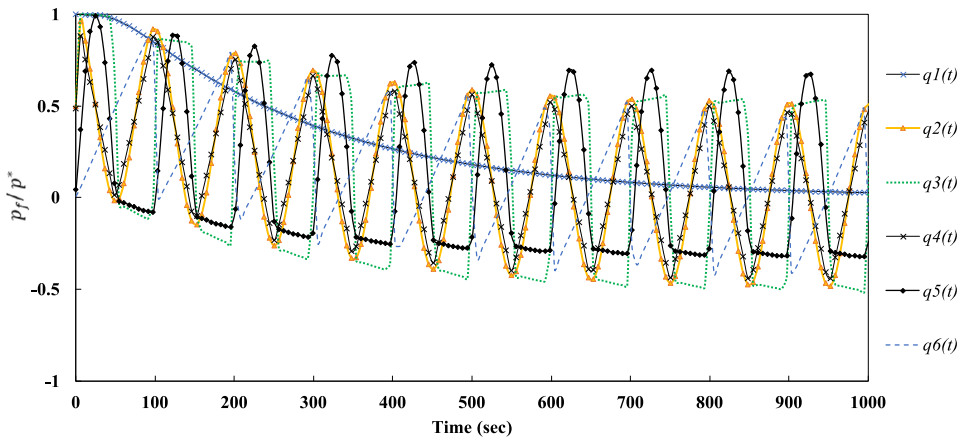

Fig. 14 A comparison of the results of dimensionless excess pore water pressure with time for saturated silty clay soil under constant type load $q_1(t)$, cosine-wave type cyclic load $q_2(t)$, square-wave type cyclic load $q_3(t)$, triangle-wave type cyclic load $q_4(t)$, half-rectified sine wave type cyclic load $q_5(t)$, and saw tooth-wave type cyclic load $q_6(t)$

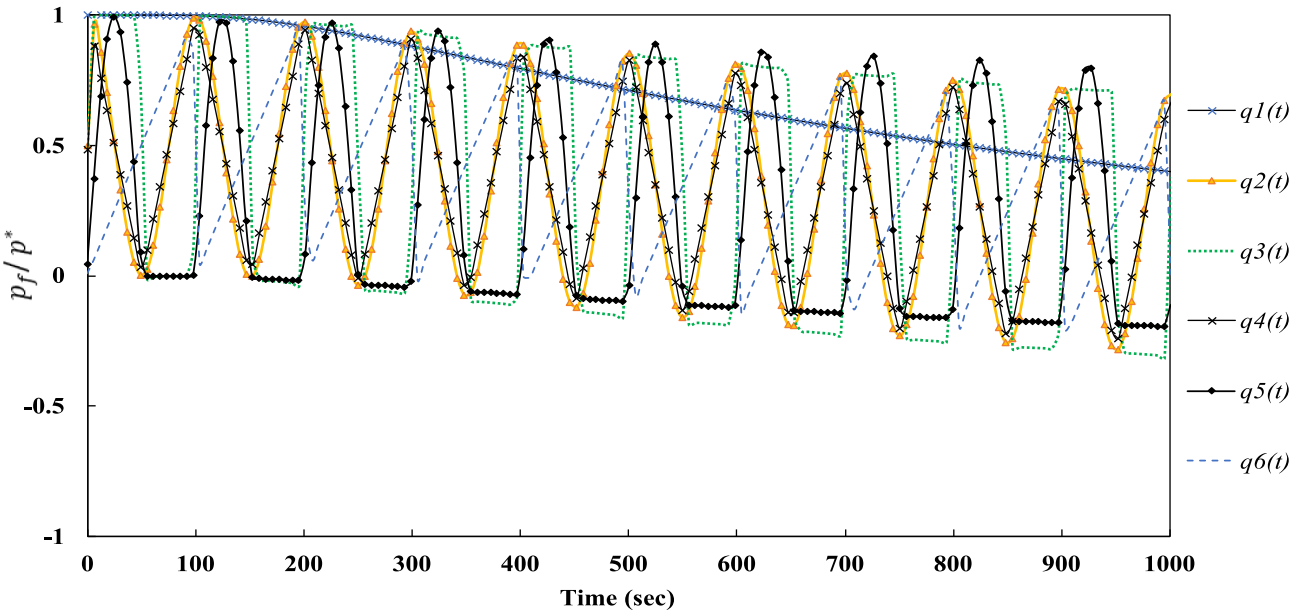

Fig. 15 A comparison of the results of dimensionless excess pore water pressure with time for saturated clay soil under constant type load $q_1(t)$, cosine-wave type cyclic load $q_2(t)$, square-wave type cyclic load $q_3(t)$, triangle-wave type cyclic load $q_4(t)$, half-rectified sine wave type cyclic load $q_5(t)$, and saw tooth-wave type cyclic load $q_6(t)$

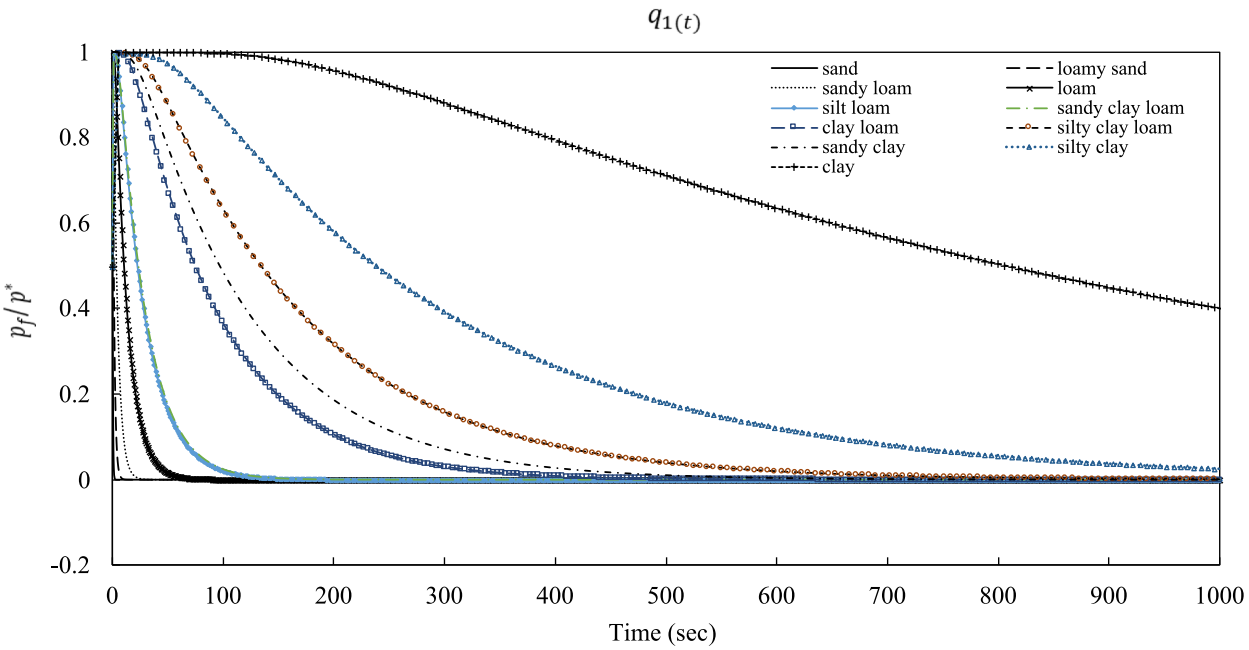

Fig. 16 A comparison of the results of dimensionless excess pore water pressure with time for 11 different types of saturated soils under constant load $q_1(t)$

4 Conclusion and Recommendations

In this study, an effective unified approach is utilized to solve the one-dimensional consolidation equation for various time-dependent loads. The novelty of this study is to employ the CFM together with the Laplace transformation and modified Durbin's inverse transformation in the solution of the considered problem. This approach is employed for the first time in geotechnical engineering. By following this approach, we successfully obtained the related canonical governing equations for the first time.

The results of this study show excellent agreement when compared with those existing in the available literature. Consequently, the proposed method has been validated as effective and successful in solving the canonical equations governing the one-dimensional consolidation of soils under time-dependent loading. Different soil types under various loads are examined to obtain the results of excess pore water pressure, and a program is coded for this purpose. The findings demonstrate that:

- The curve of the dimensionless excess pore water pressure with time variation obtained for clay soil under the constant load $q_1(t)$ resembles Terzaghi's exact solution, thereby validating the effectiveness of the proposed method.
- When the effect of soil properties on consolidation is examined, it has been observed that the dimensionless excess pore water pressure value gradually decreases over time in different soil types under constant load $q_1(t)$.
- It has been noted that under various cyclic loads, sand soil exhibits a less periodic response compared to other soils, while clay soil demonstrates a more pronounced periodic response to the excess pore water pressure.
- In terms of the load functions for sand and loamy sand soils, the square wave type yielded the highest values of dimensionless excess pore water pressure.
- For sandy loam soil, the values of dimensionless excess pore water pressure under the half-rectified sine wave type are highest and closely match those under the square wave type.
- The half-rectified sine wave type created the greatest values of p_f/p^* for loam, silt loam, sandy clay loam, clay loam, silty clay loam, sandy clay, and silty clay soils. In clay soil, the load graphs of p_f/p^* values oscillated at approximately the same values.
- Results demonstrate that type of the soil has a crucial role in determining its dynamic behavior. It is recommended that if the solid is subjected to dynamic loads the engineers should make a detailed analysis of consolidation.
- The suggested method can be applied for any arbitrary dynamic load.
- It is believed that the results of this paper can be used as benchmark solutions for the future research studies in this field.

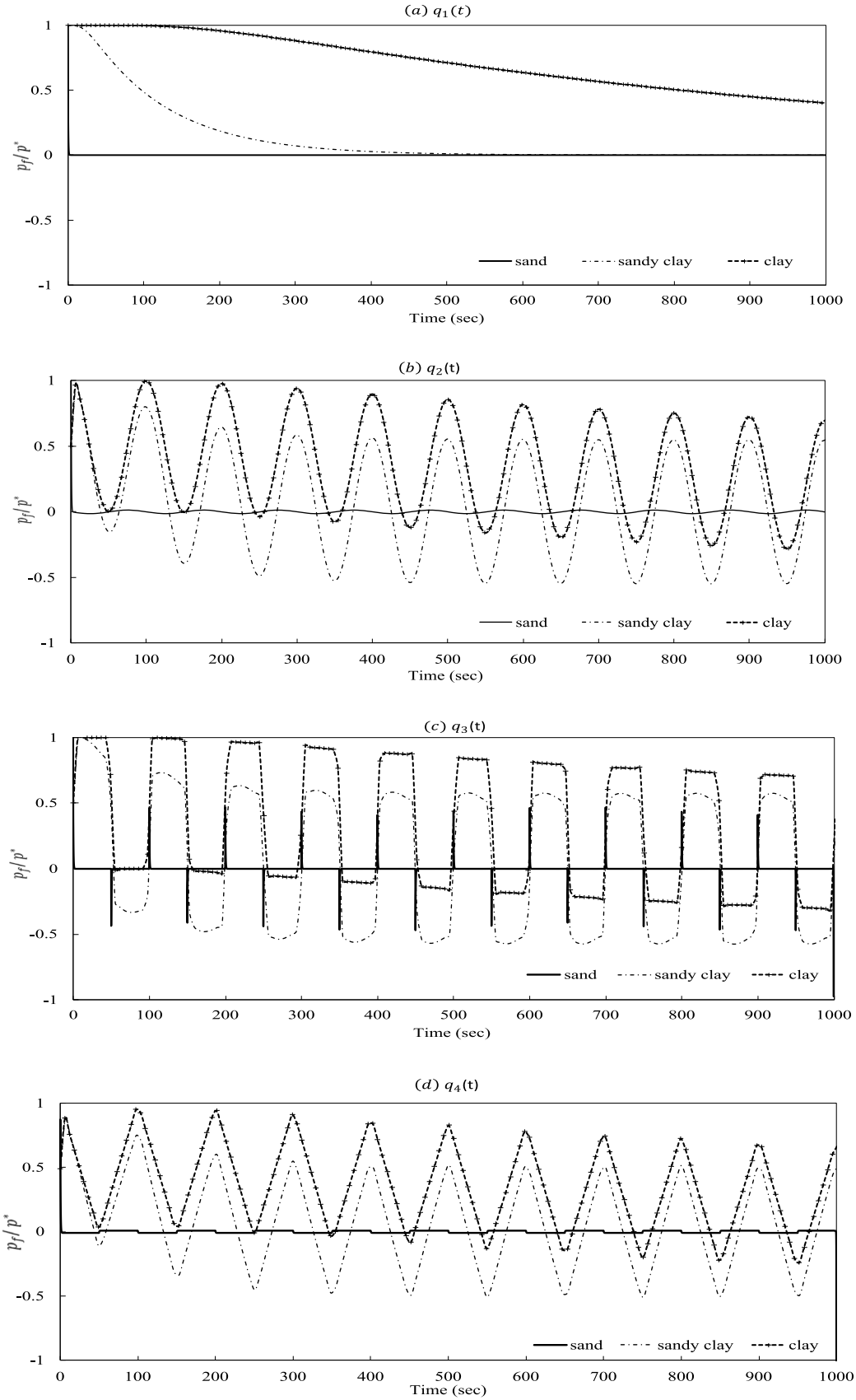

Fig. 17 p_f/p^* values with time for saturated sand, sandy clay, and clay soil under external time-varying loads **a** constant load $q_1(t)$, **b** cosine-wave type cyclic load $q_2(t)$, **c** square-wave type cyclic load $q_3(t)$, and **d** triangle-wave type cyclic load $q_4(t)$

Funding Open access funding provided by the Scientific and Technological Research Council of Türkiye (TÜBİTAK).

References

1. Terzaghi, K.: Principles of soil mechanics. IV. Settlement and consolidation of clay. Eng. News-Record. 95, 874 (1925).
2. Karl, T.: Theoretical soil mechanics, (1943).
3. Schiffman, R.L.: Consolidation of soil under time-dependent loading and varying permeability. In: Highw. Res. Board Proc. pp. 584–617. National Academy of Sciences Washington, DC (1958).
4. Radhika, B.P.; Krishnamoorthy, A.; Rao, A.U.: A review on consolidation theories and its application. Int. J. Geotech. Eng. **14**, 9–15 (2020). https://doi.org/10.1080/19386362.2017.1390899
5. Wilson, N.E.; Elgohary, M.M.: Consolidation of soils under cyclic loading. Can. Geotech. J. **11**, 420–423 (1974). https://doi.org/10.1139/t74-042
6. Xu, L.; Yuan-qiang, C.; Shi-ming, W.: Study on one-dimensional consolidation of saturated soil with semi-pervious boundaries and under cyclic loading. J. Zhejiang Univ. A. **3**, 513–519 (2002). https://doi.org/10.1631/jzus.2002.0513
7. Yuan-qiang, C.; Xu, L.; Shi-ming, W.: One-dimensional consolidation of layered soils with impeded boundaries under time-dependent loadings. Appl. Math. Mech. **25**, 937–944 (2004). https://doi.org/10.1007/BF02438802
8. Ying-chun, Z.; Kang-he, X.: Study on one-dimensional consolidation of soil under cyclic loading and with varied compressibility. J. Zhejiang Univ. A. **6**, 141–147 (2005). https://doi.org/10.1631/BF02847978
9. Xie, K.; Qi, T.; Dong, Y.: Nonlinear analytical solution for one-dimensional consolidation of soft soil under cyclic loading. J. Zhejiang Univ. A. **7**, 1358–1364 (2006). https://doi.org/10.1631/jzus.2006.A1358
10. Cai, Y.-Q.; Geng, X.-Y.; Xu, C.-J.: Solution of one-dimensional finite-strain consolidation of soil with variable compressibility under cyclic loadings. Comput. Geotech. **34**, 31–40 (2007). https://doi.org/10.1016/j.compgeo.2006.08.008
11. Lo, W.; Borja, R.I.; Chao, N.; Liu, Y.; Lee, J.: Poroelastic response of unsaturated soils to cyclic loads with arbitrary waveforms. Int. J. Numer. Anal. Methods Geomech. **48**, 679–700 (2024). https://doi.org/10.1002/nag.3659
12. Kim, P.; Kim, H.-S.; Pak, C.-U.; Paek, C.-H.; Ri, G.-H.; Myong, H.-B.: Analytical solution for one-dimensional nonlinear consolidation of saturated multi-layered soil under time-dependent loading. J. Ocean Eng. Sci. **6**, 21–29 (2021). https://doi.org/10.1016/j.joes.2020.04.004
13. Liu, J.; Ma, Q.: One-dimensional consolidation of soft ground with impeded boundaries under depth-dependent ramp load. In: Pav. and geot. eng. for transportation. pp. 127–134 (2013). https://doi.org/10.1061/9780784412817.0
14. Sivakugan, N.; Lovisa, J.; Ameratunga, J.; Das, B.M.: Consolidation settlement due to ramp loading. Int. J. Geotech. Eng. **8**, 191–196 (2014). https://doi.org/10.1179/1939787913Y.0000000017
15. Xie, K.-H.; Huang, D.-Z.; Wang, Y.-L.; Deng, Y.-B.: Analytical theory for one-dimensional consolidation of soil induced by time-dependent pumping and loading. Mar. Georesources Geotechnol. **32**, 328–350 (2014). https://doi.org/10.1080/1064119X.2013.764555
16. Hawlader, B.C.; Muhunthan, B.; Imai, G.: Viscosity effects on one-dimensional consolidation of clay. Int. J. Geomech. **3**, 99–110 (2003). https://doi.org/10.1061/(ASCE)1532-3641(2003)3:1(99
17. Satwik, C.S.; Chakraborty, M.: Numerical analysis of one-dimensional consolidation of soft clays subjected to cyclic loading and non-Darcian flow. Comput. Geotech. **146**, 104742 (2022). https://doi.org/10.1016/j.compgeo.2022.104742
18. Müthing, N.; Razouki, S.S.; Datcheva, M.; Schanz, T.: Rigorous solution for 1-D consolidation of a clay layer under haversine cyclic loading with rest period. Springerplus **5**, 1–13 (2016). https://doi.org/10.1186/s40064-016-3660-9
19. Razouki, S.S.; Schanz, T.: One-dimensional consolidation under haversine repeated loading with rest period. Acta Geotech. **6**, 13–20 (2011). https://doi.org/10.1007/s11440-010-0132-1
20. Chai, J.-C.; Shen, S.-L.; Wang, J.; Liu, M.D.: Intermittent cyclic load induced 1D consolidation settlement. Transp. Geotech. **36**, 100814 (2022). https://doi.org/10.1016/j.trgeo.2022.100814
21. Cai, Y.; Geng, X.: Consolidation analysis of a semi-infinite transversely isotropic saturated soil under general time-varying loadings. Comput. Geotech. **36**, 484–492 (2009). https://doi.org/10.1016/j.compgeo.2008.08.014
22. Ding, P.; Xu, R.; Ju, L.; Qiu, Z.; Cheng, G.; Zhan, X.: Semi-analytical analysis of fractional derivative rheological consolidation considering the effect of self-weight stress. Int. J. Numer. Anal. Methods Geomech. **45**, 1049–1066 (2021)
23. Wang, L.; Sun, D.; Li, P.; Xie, Y.: Semi-analytical solution for one-dimensional consolidation of fractional derivative viscoelastic saturated soils. Comput. Geotech. **83**, 30–39 (2017). https://doi.org/10.1016/j.compgeo.2016.10.020
24. Xu, X.-B.; Cui, Z.-D.: Investigation of one-dimensional consolidation of fractional derivative model for viscoelastic saturated soils caused by the groundwater level change. KSCE J. Civ. Eng. **26**, 4997–5009 (2022). https://doi.org/10.1007/s12205-022-1949-5
25. Huang, M.; Lv, C.; Zhou, S.; Zhou, S.; Kang, J.: One-dimensional consolidation of viscoelastic soils incorporating caputo-fabrizio fractional derivative. Appl. Sci. **11**, 927 (2021). https://doi.org/10.3390/app11030927
26. Wang, H.; Chen, Y.; Huang, B.: Computation of one-dimensional consolidation of double layered ground using differential quadrature method. J. Zhejiang Univ. A. **4**, 195–201 (2003). https://doi.org/10.1631/jzus.2003.0195
27. Xie, K.H.: Theory of one dimensional consolidation of double-layered ground and its applications. Chinese J. Geotech. Eng. **16**(5), 24–35 (1994)
28. Xie, J.; Wen, M.; Gao, Z.; Wu, D.; Yu, D.; Zhang, X.; Lou, S.; Wan, J.: An interfacial flow contact model for 2D plane strain consolidation analysis of layered saturated soil under continuous drainage boundaries. Comput. Geotech. **179**, 106993 (2025). https://doi.org/10.1061/(ASCE)GM.1943-5622.0002300
29. Zhao, X.; Liu, Y.; Cao, W.; Gong, W.: Semi-analytical solution for two-dimensional electro-osmotic consolidation of double-layered soil. Geotext. Geomembranes. **52**, 121–131 (2024). https://doi.org/10.1016/j.geotexmem.2023.09.007

30. Tian, Y.; Jiang, G.; Gui, Y.; Wen, M.; Mei, G.; Wu, W.; Zhang, Y.: A semi-analytical model for coupled THM consolidation of saturated clays improved by PVTD considering thermal contraction. Int. J. Numer. Anal. Methods Geomech. **48**, 2900–2924 (2024). https://doi.org/10.1002/nag.3758
31. Chung, S.G.; Kweon, H.J.; Chung, C.G.: Back-analysis of one-dimensional consolidation settlement. Acta Geotech. **19**(1), 239–254 (2024). https://doi.org/10.1007/s11440-023-01964-8
32. Olek, B.S.: State-of-the-Art Review on determining one-dimensional consolidation parameters based on compression and distribution of pore water pressure: coefficient of consolidation (cv), end of primary (eop) consolidation. Arch. Comput. Method E (2024). https://doi.org/10.1007/s11831-024-10154-y
33. Sadeghian, R.; Maleki, M.; Kazempour, A.: Laboratory investigation of the swelling pressure of bentonite with quicklime and hydrated lime using ASTM-4546-96 and constant volume methods. Sci. Rep. **14**(1), 21223 (2024). https://doi.org/10.1038/s41598-024-72143-2
34. Tuc, E.; Akbas, S.O.; Babagiray, G.: Reliability and validity analysis of correlations on strength and consolidation parameters for Ankara clay and proposal for a new correlation. Arab. J. Sci. Eng. (2024). https://doi.org/10.1007/s13369-024-09181-5
35. Arab, M.; Benessalah, I.; Hage Chehade, F.; Arab, A.: One-dimensional consolidation and stress–strain behaviour of chlef or standard granular sand mixed with bentonite. Arab. Arab. J. Sci. Eng. (2025). https://doi.org/10.1007/s13369-025-09961-7
36. Singh, A.; Chakraborty, M.: Combined effect of non-darcian flow and semipermeable drainage boundaries on one-dimensional consolidation of unsaturated Soil. Int. J. Geomech. **24**(8), 04024157 (2024). https://doi.org/10.1061/IJGNAI.GMENG-9659
37. Deng, J.-H.; Lee, J.-W.; Lo, W.: Closed-form solutions for one-dimensional consolidation in saturated soils under different waveforms of time-varying external loading. J. Hydrol. **573**, 395–405 (2019). https://doi.org/10.1016/j.jhydrol.2019.03.087
38. Aslan, T.A.; Noori, A.R.; Temel, B.: An efficient approach for free vibration analysis of functionally graded sandwich beams of variable cross-section. Structures (2023). https://doi.org/10.1016/j.istruc.2023.105397
39. Calim, F.F.: Transient analysis of axially functionally graded Timoshenko beams with variable cross-section. Compos. Part B Eng. **98**, 472–483 (2016). https://doi.org/10.1016/j.compositesb.2016.05.040
40. Can, N.; Keles, I.: A practical jointed approach to transient hyperbolic heat conduction of FGM cylinders and spheres. J. Mech. Sci. Technol. **37**, 1223–1231 (2023). https://doi.org/10.1007/s12206-023-0209-z
41. Aslan, T.A.; Noori, A.R.; Temel, B.: Dynamic response of viscoelastic tapered cycloidal rods. Mech. Res. Commun. **92**, 8–14 (2018). https://doi.org/10.1016/j.mechrescom.2018.06.006
42. Noori, A.R.; Aslan, T.A.; Temel, B.: Damped transient response of in-plane and out-of-plane loaded stepped curved rods. J. Braz. Soc. Mech. Sci. Eng. **40**, 1–25 (2018). https://doi.org/10.1007/s40430-017-0949-8
43. Noori, A.R.; Temel, B.: On the vibration analysis of laminated composite parabolic arches with variable cross-section of various ply stacking sequences. Mech. Adv. Mater. Struct. **27**, 1658–1672 (2020). https://doi.org/10.1080/15376494.2018.1524949
44. Rasooli, H.; Noori, A.R.; Temel, B.: Static analysis of functionally graded porous beam-column frames by the complementary functions method. Structures (2024). https://doi.org/10.1016/j.istruc.2024.106136
45. Temel, B.; Aslan, T.A.; Noori, A.R.: In-plane vibration analysis of parabolic arches having a variable thickness. Int. J. Dyn. Control. **9**, 910–921 (2021). https://doi.org/10.1007/s40435-020-00727-7
46. Temel, B.; Noori, A.R.: Out-of-plane vibrations of shear-deformable AFG cycloidal beams with variable cross section. Appl. Acoust. **155**, 84–96 (2019). https://doi.org/10.1016/j.apacoust.2019.05.010
47. Temel, B.; Yildirim, S.; Tutuncu, N.: Elastic and viscoelastic response of heterogeneous annular structures under arbitrary transient pressure. Int. J. Mech. Sci. **89**, 78–83 (2014). https://doi.org/10.1016/j.ijmecsci.2014.08.021
48. Yildirim, S.: Hydrogen elasticity solution of functionally-graded spheres, cylinders and disks. Int. J. Hydrogen Energy **45**, 22094–22101 (2020). https://doi.org/10.1016/j.ijhydene.2020.05.272
49. Biot, M.A.: General theory of three-dimensional consolidation. J. Appl. Phys. **12**, 155–164 (1941)
50. Biot, M.A.: Theory of propagation of elastic waves in a fluid-saturated porous solid. II. Higher frequency range. J. Acoust. Soc. Am. **28**(2), 179–191 (1956)
51. Biot, M.A.: Mechanics of deformation and acoustic propagation in porous media. J. Appl. Phys. **33**, 1482–1498 (1962)
52. Ausilio, E.; Conte, E.: Settlement rate of foundations on unsaturated soils. Can. Geotech. J. **36**, 940–946 (1999)
53. Fredlund, D.G.; Hasan, J.U.: One-dimensional consolidation theory: unsaturated soils. Can. Geotech. J. **16**, 521–531 (1979)
54. Zheng-Han, C.: Consolidation theory of unsaturated soil based on the theory of mixture (II). Appl. Math. Mech. **14**, 721–733 (1993)
55. Lo, W.-C.; Sposito, G.; Chu, H.: Poroelastic theory of consolidation in unsaturated soils. Vadose Zo. J. **13**, 1–12 (2014)
56. Lovisa, J.: An insight into time rate of consolidation, (2012).
57. Spiegel, M.R.: Laplace transforms. McGraw-Hill New York (1965).
58. Lo, W.-C.; Sposito, G.; Lee, J.-W.; Chu, H.: One-dimensional consolidation in unsaturated soils under cyclic loading. Adv. Water Resour. **91**, 122–137 (2016). https://doi.org/10.1016/j.advwatres.2016.03.001
59. Chao, N.-C.; Lee, J.-W.; Lo, W.: Gravity effect on consolidation in poroelastic soils under saturated and unsaturated conditions. J. Hydrol. **566**, 99–108 (2018). https://doi.org/10.1016/j.jhydrol.2018.08.081
60. Lo, W.-C.; Yeh, C.-L.; Tsai, C.-T.: Effect of soil texture on the propagation and attenuation of acoustic wave at unsaturated conditions. J. Hydrol. **338**, 273–284 (2007). https://doi.org/10.1016/j.jhydrol.2007.02.034
61. Lo, W.-C.; Yeh, C.-L.; Jan, C.-D.: Effect of soil texture and excitation frequency on the propagation and attenuation of acoustic waves at saturated conditions. J. Hydrol. **357**, 270–281 (2008). https://doi.org/10.1016/j.jhydrol.2008.05.018
62. Rawls, W.J.; Ahuja, L.R.; Brakensiek, D.L.: Estimating soil hydraulic properties from soils data. Indirect Methods Estim. Hydraul. Prop. Unsaturated Soils **32**(9), 329–340 (1992). https://doi.org/10.1007/978-1-4612-3144-8_5